Journal of Translational Medicine

RESEARCH

Open Access

Spastin accumulation and motor neuron defects caused by a novel *SPAST* splice site mutation

Min Luo[1], Yanying Wang[1], Jinxiu Liang[2] and Xinhua Wan[1*]

Abstract

Background Hereditary spastic paraplegia (HSP) is a rare genetically heterogeneous neurodegenerative disorder. The most common type of HSP is caused by pathogenic variants in the *SPAST* gene. Various hypotheses regarding the pathogenic mechanisms of HSP-SPAST have been proposed. However, a single hypothesis may not be sufficient to explain HSP-SPAST.

Objective To determine the causative gene of autosomal dominant HSP-SPAST in a pure pedigree and to study its underlying pathogenic mechanism.

Methods A four-generation Chinese family was investigated. Genetic testing was performed for the causative gene, and a splice site variant was identified. In vivo and in vitro experiments were conducted separately. Western blotting and immunofluorescence were performed after transient transfection of cells with the wild-type (WT) or mutated plasmid. The developmental expression pattern of zebrafish *spasts* was assessed via whole-mount in situ hybridization. The designed guide RNA (gRNA) and an antisense oligo *spast*-MO were microinjected into *Tg(hb9:GFP)* zebrafish embryos, spinal cord motor neurons were observed, and a swimming behavioral analysis was conducted.

Results A novel heterozygous intron variant, c.1004 + 5G > A, was identified in a pure HSP-SPAST pedigree and shown to cosegregate with the disease phenotypes. This intron splice site variant skipped exon 6, causing a frameshift mutation that resulted in a premature termination codon. In vitro, the truncated protein was evenly distributed throughout the cytoplasm, formed filamentous accumulations around the nucleus, and colocalized with microtubules. Truncated proteins diffusing in the cytoplasm appeared denser. No abnormal microtubule structures were observed, and the expression levels of α-tubulin remained unchanged. In vivo, zebrafish larvae with this mutation displayed axon pathfinding defects, impaired outgrowth, and axon loss. Furthermore, *spast*-MO larvae exhibited unusual behavioral preferences and increased acceleration.

Conclusion The adverse effects of premature stop codon mutations in SPAST result in insufficient levels of functional protein, and the potential toxicity arising from the intracellular accumulation of spastin serves as a contributing factor to HSP-SPAST.

Keywords Hereditary spastic paraplegia, HSP, Spastin, Microtubule severing

*Correspondence:
Xinhua Wan
wanxh@pumch.cn

[1]Department of Neurology, Peking Union Medical College, Peking Union Medical College Hospital, Chinese Academy of Medical Science, Beijing 100730, China
[2]Center for Genetic Medicine, The Fourth Affiliated Hospital, Zhejiang University School of Medicine, Hangzhou 310000, Zhejiang, China

Introduction

Hereditary spastic paraplegia (HSP) is a rare genetically heterogeneous disorder characterized by progressive degeneration of the corticospinal tracts [1].

The average global prevalence of HSP is 1.27 to 9.8 per 100,000 people, with well over 80 distinct genetic loci reported [2]. HSP is clinically classified into pure and complicated forms. Pure HSP primarily presents as lower extremity spasticity, weakness, and neurogenic bladder dysfunction. Complicated HSP is accompanied by additional neurological or systemic abnormalities, including seizures, ataxia, parkinsonism, and cognitive decline [3–6]. HSP inheritance patterns can be autosomal dominant (AD), autosomal recessive (AR), X-linked recessive, or mitochondrial. AD-HSP is the predominant form of the disease, accounting for 43–80% of cases [3, 7–11].

Spastic paraplegia type 4 (SPG4) is the most common type of AD-HSP and is caused by a pathogenic variant in *SPAST.* Most HSP-SPAST patients are clinically characterized as pure HSPs [12–14]. The *SPAST* gene is located on chromosome 2p22.3 and encodes a microtubule-severing ATPase called spastin. Most pathogenic variants in HSP-SPAST are nonsense, missense, or splice site mutations or insertions [15]. Mutations in spastin affect microtubule severity and dynamics, calcium homeostasis via store-operated calcium entry (SOCE), remodeling of the endoplasmic reticulum (ER) in axons, and movement of lipid droplets along microtubules [16–19].

Most research has suggested that haploinsufficiency is the underlying molecular mechanism of this disease [20]. However, truncated mutations in HSP-SPAST patients cannot be fully explained by loss-of-function mechanisms. Nonsense-mediated mRNA decay (NMD) is an mRNA degradation pathway in which transcripts carrying premature termination codons (PTCs) are degraded. NMD is believed to inhibit the synthesis of toxic truncated proteins [21]. However, studies on the half-lives of mRNAs containing PTCs have demonstrated that the efficiency of NMD varies across transcripts, cells, tissues, and individuals; not all cells degrade all of the mRNAs, and some can escape degradation [22]. Abnormal aggregation and toxic gain-of-function mechanisms may also be involved.

In our study, we investigated a four-generation Chinese family with HSP-SPAST and identified a novel variant, c.1004+5G>A (NM_014946.4), in the *SPAST* gene that produces a truncated protein. Functional studies of the novel variant found that the truncated spastin protein exhibited filamentous expression. Furthermore, we generated *spast*-E6I6-MO and *spast*-F_0 crispant zebrafish models that exhibited spinal motor neuron axon pathfinding defects, and the acceleration of *spast*-MO larvae was greater than that of *std*-MO larvae.

In summary, we propose that the adverse effects of this novel mutation are attributed to insufficient levels of functional protein. The potential toxicity caused by the intracellular accumulation of spastin is considered a contributing factor to HSP-SPAST.

Materials and methods

Subjects

SPAST-HSP patients were examined and diagnosed at the Department of Neurology, Peking Union Medical College Hospital (PUMCH). Their relatives were also recruited for this study. Genomic DNA was extracted from peripheral blood using a QIAamp DNA Blood Kit (QIAGEN, Hilden, Germany). Whole-exome sequencing was performed for the proband. The proband and available relatives from the family were tested for mutation segregation by Sanger sequencing. Disease severity was assessed using the Spastic Paraplegia Rating Scale (SPRS) [23]. Informed consent was obtained from all participants. This study received approval from the ethics committees of PUMCH and adhered to the principles of the Declaration of Helsinki.

Splice variant analysis

Whole blood was collected from four case subjects in PAXgene Blood RNA tubes. RNA extraction was performed using the PAXgene Blood RNA Kit (QIAGEN, Hilden, Germany) following the manufacturer's instructions. Blood total RNA was reverse transcribed to cDNA using EasyScript® First-Strand cDNA Synthesis SuperMix for RT−PCR (TransGen, Beijing, China). Specific primers (SPAST-E5-9-F-490 bp: F: 5′-CACTGCCTCGTTCAAAAACA-3′; R: 5′-GCACTTATATTAAAGAAGGTTGCATT-3′) were designed to amplify the region surrounding the relevant cDNA fragment. Polymerase chain reaction (PCR) products were analyzed by agarose gel electrophoresis and compared to control samples, and the purified PCR products were subsequently subjected to Sanger sequencing (ABI 3730XL DNA, Thermo Fisher Scientific, USA).

Plasmid construction

The full-length SPAST cDNA sequence (NM_014946-3flag) and the mutation plasmid sequence (NM_014946(c.del871-1004)-3flag), obtained by deleting exon 6 from the full-length *SPAST* gene, were cloned and inserted into Vector Gv657. The short-length plasmids NM_014946 (c.del871-1004, del1016-1848)-3flag and 3flag-NM_014946 (c.del871-1004), both of which were edited based on full-length *SPAST* cDNA, were cloned and inserted into Vector Gv658. All wild-type and mutant vectors were confirmed by Sanger sequencing.

Cell culture and transfection

HEK293T and HeLa cells were cultured in Dulbecco's modified Eagle's medium (DMEM)/MEM supplemented with 10% fetal bovine serum (FBS) and 1× penicillin/streptomycin (all from Gibco, Grand Island, NY, USA) and incubated at 37 °C in 5% CO_2. Transfection-positive cells were identified by ZsGreen. The plasmids were transfected using Lipofectamine 3000 (Invitrogen, Carlsbad, CA, USA). At 48 h after transfection, the transfected cells were collected for further analysis.

Western blotting

Transfected HEK293T cells were lysed with RIPA buffer containing protease (AQ, AQ521) and phosphatase inhibitor cocktail (AQ, AQ551). The protein concentration was assessed using bicinchoninic acid (BCA) (Thermo Scientific). The protein samples were separated on 4%~12% polyacrylamide gels (ACE, ET15412LGel) and transferred onto polyvinylidene fluoride (PVDF) membranes. The membranes were incubated with primary antibodies overnight at 4 °C. The antibodies used in this study were anti-Flag (Abcam, ab150083), anti-tubulin (Proteintech, ab7291), and anti-GAPDH (Protein Tech, 60004-1-Ig). Next, the membranes were incubated with secondary antibodies.

Immunofluorescence

At 48 h post-transfection, HEK293T and HeLa cells were fixed with 4% paraformaldehyde and then treated with 0.5% Triton X-100 at room temperature. After blocking with 1% bovine serum albumin (BSA; Sigma−Aldrich) for 40 min, the cells were incubated with anti-α-tubulin antibodies (Proteintech, ab7291) overnight at 4 °C. Following primary antibody incubation, the slides were washed before being incubated for 1 h at room temperature with Alexa Fluor 594-conjugated rabbit antibodies (Proteintech, SA00013-4). The nuclei were stained with 4,6-diamidino-2-phenylindole (DAPI). Images were acquired using an LSM 980 system with an Airyscan 2 - Confocal Microscope (Zeiss, Germany).

Zebrafish maintenance

Wild-type AB and transgenic *Tg(hb9:GFP)* zebrafish (*Danio rerio*) lines were obtained from EzeRinka and reared in a recirculating system at 28.5 ℃ under a 14-h light/10-h dark cycle. Embryos created through natural mating were collected from six pairs of zebrafish at the 1-cell stage and cultured at 28.5 °C in E3 media (5 mM NaCl, 0.17 mM KCl, 0.33 mM $CaCl_2$, 0.33 mM $MgSO_4$, and 0.00001% methylene blue). All zebrafish handling and experimental procedures were approved by the Institutional Animal Care and Use Committee of Zhejiang University.

Table 1 Zebrafish primers and target sequences for gRNA

CRISPR gRNA	gRNA target sequence	qPCR forward (F) and reverse (*R*) primers
Target1	TGACGCAGTGGCAGTGGTAC TGG	F: AGAAGGTTTG TCTCACAGGGTC R: AACTGCAATAT GCACCTAAACC
Target2	CCTCATCCTCAACGAGATCG TGG	
Target3	CCACGATCTCGTTGAGGATG AGG	
Target4	TCCTCAACGAGATCGTGGAC AGG	

Guide RNA design and crispant mutagenesis

Guide RNA (gRNA) for *spast* gene targets, along with primers and probes (Table 1), was synthesized following the manufacturer's manual (Precision gRNA Synthesis Kit, Thermo Fisher Scientific). A mixed solution containing 320 ng/μL gRNA, 800 ng/μL Cas9 nuclease (EnGen® Spy Cas9 NLS, M0646T, NEB, USA) and phenol red dye (Sigma, P0290) was prepared. Microinjections were carried out in zebrafish at the 1-cell stage, with 1 nL injected per embryo and approximately 100 embryos per target site. Twenty F_0 crispant larvae (3 dpf) from each group were randomly selected for ethanol precipitation DNA extraction, PCR amplification, and Sanger sequencing. The PCR products were recycled (TIANGEN, DP204-03, Beijing, China) and subjected to TA cloning using the Hieff Clone® Zero TOPO-TA Cloning Kit (YEASEN, 10907ES50, China) according to the manufacturer's instructions, and the target cleavage efficiency was calculated by Sanger sequencing.

Morpholino concentration test and microinjection

The *spast*-E6I6-morpholino (MO) skipping sequence (5′- ATGTTTCTAACTCTACCTGTCCACG −3′) and standard control MO sequence (5′- CCTCTTACCTC AGTTACAATTTATA-3′) were designed by GeneTools (Philomath, Oregon, USA). Microinjection was performed into 1-cell stage embryos at concentrations of 4 ng/nL, 8 ng/nL, 12 ng/nL, and 16 ng/nL per 200 embryos according to standard procedures. Subsequently, total RNA from each group was extracted from 20 larvae at 2 days postfertilization (dpf) using TRIzol™ reagent (Thermo Fisher Scientific) and reverse transcribed into cDNA with Thermo Scientific RevertAid RT. RT−PCR using SYBR Green Fluorescence (Roche Diagnostics, Basel, Switzerland) was performed to test the knockdown efficiency as recommended by the manufacturer's guidelines. The specific primers used were as follows: F1, 5′-C AGCAAACTGGCAAGCCTCAT-3′; R1, 5′-CGTAGGG CAGGCAGGATGAC-3′.

Whole-mount in situ hybridization

Whole-mount in situ hybridization was performed as previously described by Christine Thisse [24]. The antisense RNA probes used were obtained from DIG RNA Labeling Mix (Roche Applied Science, Penzberg,

Germany) for probe synthesis. The primers for the probes used were as follows: *spast* F, 5′-GAAAGCCGTCGCAA TGGAATCG-3′; *spast* R, 5′-TCATACGCCAGTCGTGT CTCCG-3′. The samples were incubated at 37 °C for 3 h. Then, 1 μL of DNase 1 was added, and the samples were incubated at 37 °C for 15 min, followed by electrophoresis. Finally, a G50 column was used to purify the DIG RNA Labeling Mix. Images were acquired with an Axio Imager. D2 microscope (Zeiss, Germany), and the images were further processed for brightness and contrast using Adobe Photoshop software (Adobe Systems, San Jose, CA, USA).

Swimming behavior analysis

For swimming behavior analysis, 6 randomly selected larvae (4 days postfertilization [dpf]) from each group were transferred to a 24-well plate containing fresh E3 buffer. The 24-well plate was placed in a DanioVision behavior recording system equipped with the associated movement tracking and analysis software (EthoVision XT, Noldus, Netherlands). The light intensity, circulating water system (observation box maintained at 28 °C), and photoperiod (light 5 min/dark 5 min/light 5 min/dark 5 min) parameters were set. Simultaneous video collection and analysis of zebrafish movement trajectories were conducted.

Statistical analysis

The data were graphically illustrated and statistically analyzed with GraphPad Prism 8 software (San Diego, CA, USA). Significant differences were determined by Student's t test or one-way analysis of variance (ANOVA) for comparisons of more than two groups with a normal distribution. The data were considered statistically significant at $P<0.05$. P values are indicated as follows: $^{*}P\leq0.05$. $^{**}P\leq0.01$. $^{***}P\leq0.001$.

Results

Clinical characteristics of patients

A four-generation Chinese family with HSP-SPAST was investigated in our study (Fig. 1A). The proband (III:2, 50 years old) experienced progressive lower limb weakness and stiffness around the age of 35. Currently, he can walk independently but presents with spasticity in both legs, hyperactivity of the tendon reflex, a positive bilateral Babinski sign, and a scissors gait. His total SPRS score was 31 points. He exhibited normal intelligence and no urinary symptoms. Whole-exome sequencing (WES) of the proband's peripheral blood showed an intronic heterozygous mutation, c.1004+5G>A, in *SPAST*. The proband's mother (II:5, 73 years old) required walking aids and exhibited urinary dysfunction but no abnormalities in intelligence. Her SPRS score was 37 points. The proband's son (IV:1, 25 years old) exhibited slight stiffness in the lower limbs that did not impact exercise or walking. Neurological examination revealed hyperreflexia and a positive bilateral Babinski sign in both lower extremities, with a total SPRS score of 2 points. Sanger sequencing confirmed the novel mutation c.1004+5G>A in intron 6 of *SPAST* (Fig. 1B).

Effect of the intron mutation c.1004 + 5G > A in *SPAST*

The RT–PCR products obtained from the RNA of four patients and control samples were examined by agarose gel electrophoresis. Three different electrophoresis bands were detected for II:5, III:2, and IV:1 (Fig. 1C). One of the bands corresponded to the correctly spliced protein, and the other band indicated an alternative splicing product. Sequence analysis confirmed that the product completely skipped exon 6. Sanger sequencing of the third band showed a nonspecific band (Fig. 1D).

A. Pedigree of an HSP-affected family with *SPAST* mutations suggesting autosomal dominant Mendelian inheritance. The HSP-affected individuals are represented by filled symbols. Circle = female; square = male; *= DNA available; open symbols = individual assumed to be healthy; strikethrough = deceased individual. The proband is marked with an arrow.
B. The novel mutation was confirmed by Sanger sequencing. The red arrow indicates the position of the *SPAST* mutation. WT, wild-type.
C. Agarose gel electrophoresis of RT–PCR fragments revealed two bands (longer and shorter) in Patients II:5, III:2, and IV:1 but only one band in Patient II:4 and three unrelated controls.
D. Sequencing chromatograms of the longer and shorter bands confirmed the deletion of exon 6 in Patients III:2, II:5 and IV:1 (Figure S1).
E. Partial alignment of SPAST protein ATPase sequences from different vertebrate species. The ATPase activity of the SPAST protein is highly conserved phylogenetically. A full alignment of the SPAST protein sequences is shown in Figure S2 in the Supplementary material.

Mutation analysis and effects of *SPAST* mutations on protein expression

The heterozygous mutation c.1004+5G>A (exon 6 deletion detected by cDNA Sanger sequencing) was identified among the HSP patients. The deletion of exon 6 led to a frameshift mutation, resulting in a PTC at the 295th amino acid of SPAST, yielding a truncated protein (Fig. 2A). To further assess the effects of the mutation, we generated wild-type (WT) and mutated plasmids (D-F, F-D, and S-F) encoding fusion proteins with the

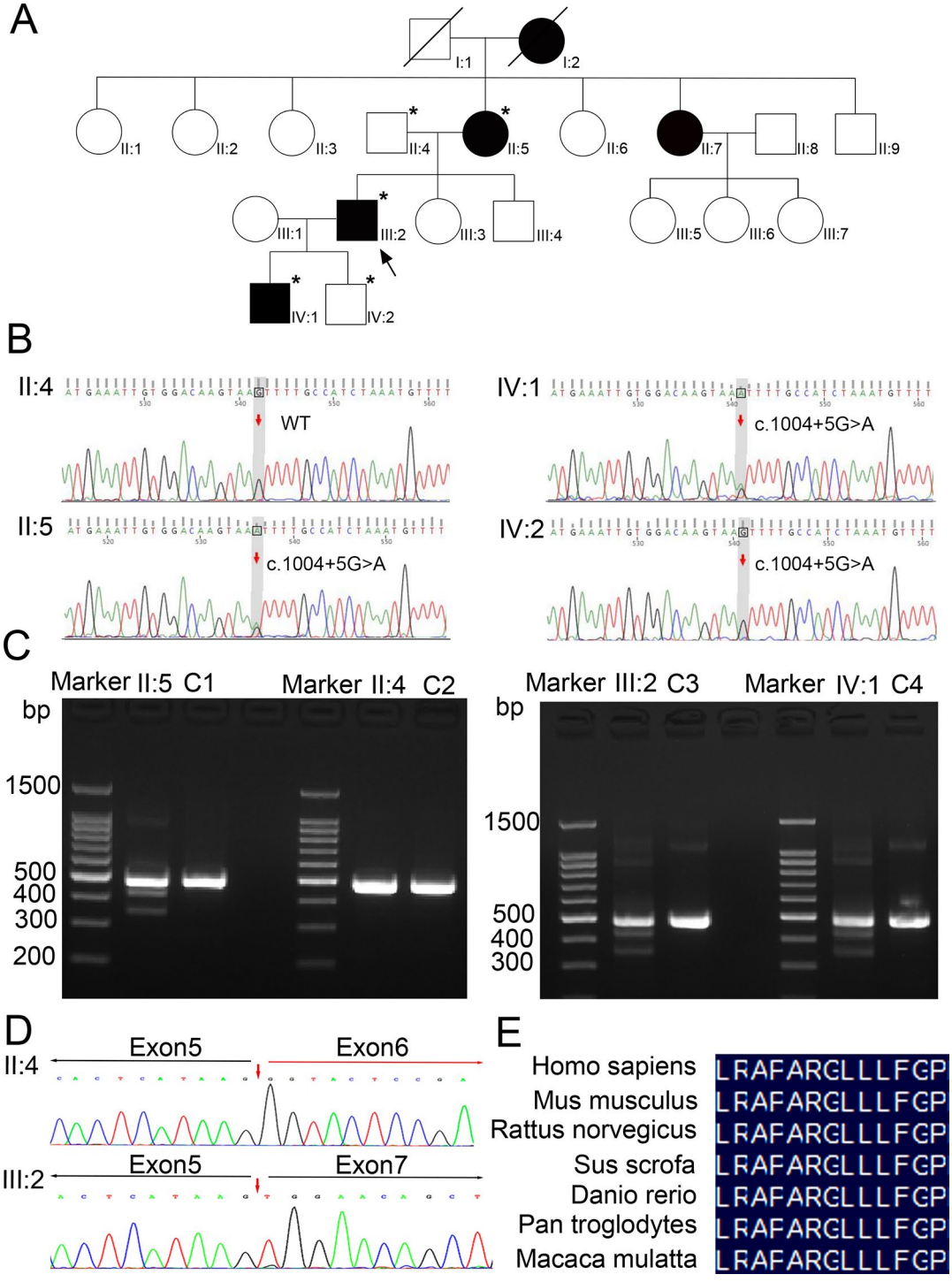

Fig. 1 Pedigree of an HSP-affected family with identified *SPAST* splicing mutations

fluorescent protein zoanthus green (ZsGreen) and the tagged protein Flag (Fig. 2B), followed by transient transfection of HEK293T cells. Full-length and truncated proteins were detected in HEK293T cells transfected with the wild-type and D-F, F-D, and S-F mutant plasmids (Fig. 2C). Western blotting analysis demonstrated greater levels of truncated Flag-tagged spastin than of wild-type spastin (Fig. 2D), with no significant difference in α-tubulin levels between the mutant and WT proteins (Fig. 2E).

A. Graphic representation of the splicing variant caused by an intronic mutation in the *SPAST* gene. The intronic variant c.1004 + 5G > A is marked by

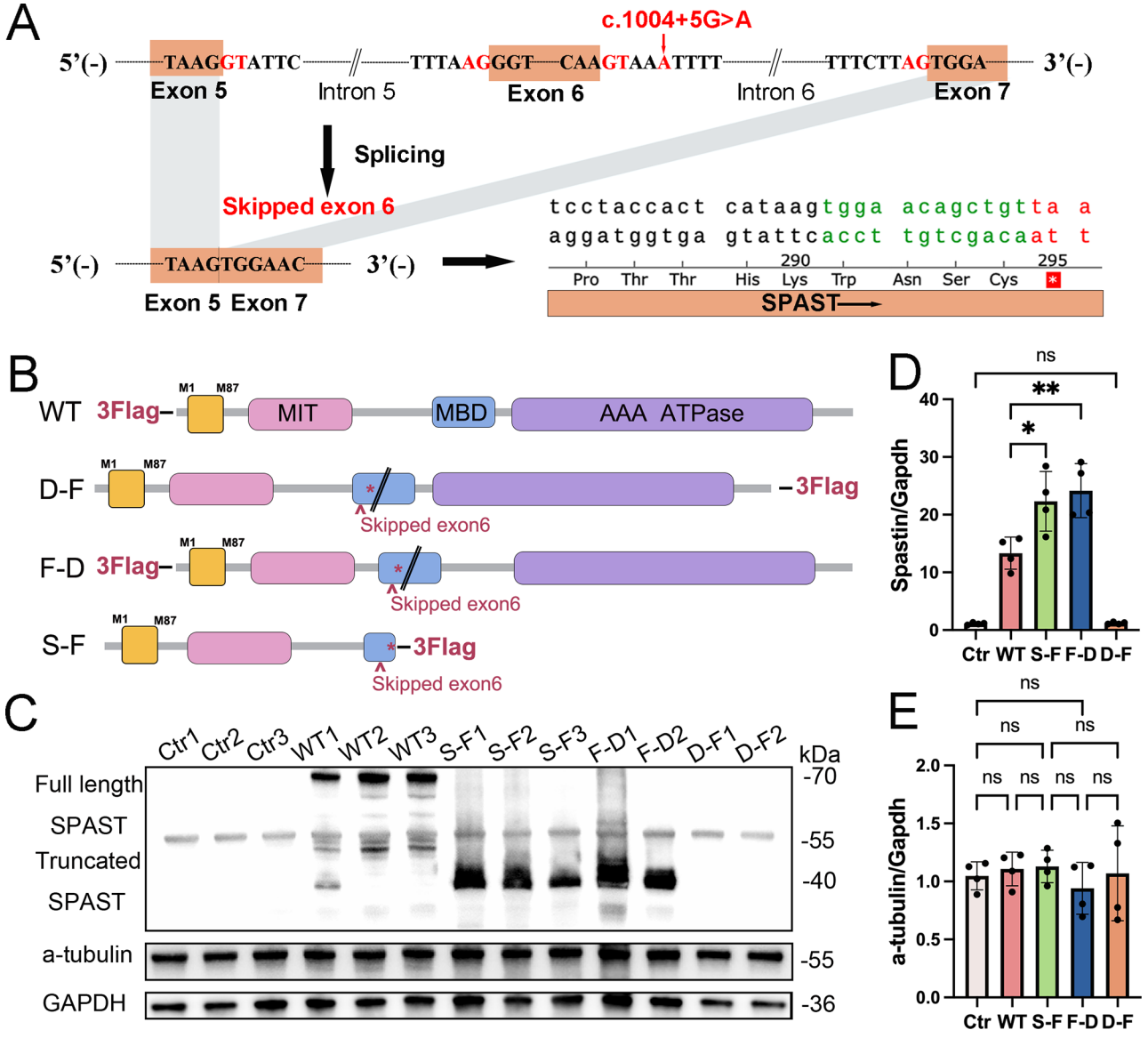

Fig. 2 Characterization of the truncated SPAST protein

a vertical red arrow. This variant caused skipping of exon 6 in the mature transcript (NM_014946.3), which created a premature termination codon at amino acid 295.

B. Schematic diagram of the human wild-type and mutant spastin proteins. MIT: microtubule interacting and trafficking domain, MBD: microtubule-binding domain, AAA: ATPase associated with various cellular activities.

C. Expression levels of the WT-spastin, truncated spastin, and a-tubulin proteins.

D. Graphical representation of spastin protein levels in (C) ($n = 4$, mean ± SD, $^{*}P \le 0.05$. $^{**}P \le 0.01$. ns: not statistically significant).

E. Graphical representation of a-tubulin levels in (C) ($n = 4$, mean ± SD, ns: not statistically significant).

Mutant protein localization and functional study

To investigate the localization of the truncated spastin protein and potential alterations caused by the mutation, ZsGreen-tagged WT and mutant plasmids were transiently transfected into HEK293T and HeLa cells. WT spastin was uniformly distributed in the cytoplasm and nucleus of HeLa cells (Fig. 3A). In contrast, the mutant truncated spastin exhibited filamentous expression and clustered deposition around the nucleus.

(Fig. 3E). Additionally, the cytoplasmic distribution of the truncated protein was greater than that of the WT

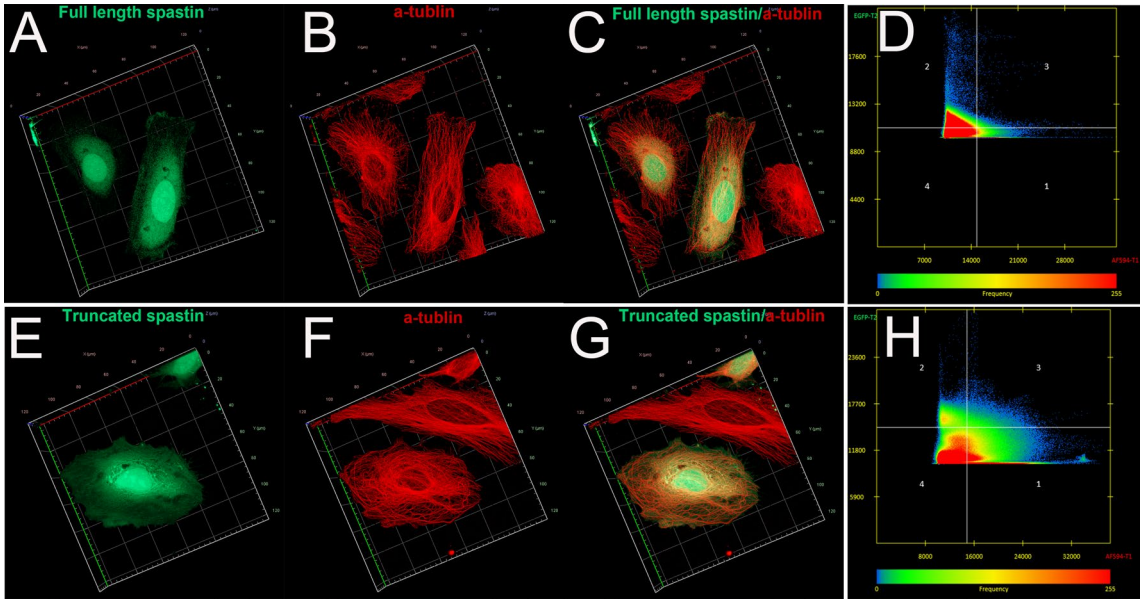

Fig. 3 Truncated spastin localization and microtubule integrity in HeLa cells. **A, E**: 3D subcellular localization of full-length and truncated spastin (green). **B, F**: 3D subcellular localization of α-tubulins (red). **C, D**: 3D full-length spastin merged with microtubules; 2D colocalization analysis. **G, H**: 3D-truncated spastin merged with microtubules; 2D colocalization analysis.

protein (Fig. 3A and E). Immunostaining of the transfected cells with an anti-α-tubulin antibody showed colocalization of filamentous truncated mutant spastin with microtubules (Fig. 3G and H). Similar observations were made in HEK293T cells (Fig. S3).

Spast expression pattern in zebrafish

Whole-mount in situ hybridization suggested that the *spast* transcript was widely expressed before 12 h postfertilization (hpf) but gradually became confined to the central nervous system, including the eye, brain, and trunk (Fig. 4). In the developing central nervous system, *spast* expression peaked at approximately 48 hpf (Fig. 4) and decreased after 72 hpf (Fig. 4).

Whole-mount in situ hybridization for *spast* in zebrafish at the 1-cell stage (A), 12 hpf (B), 24 hpf (C), 48 hpf (D), and 72 hpf (E). Dorsal and lateral views of the embryos are shown. The dotted lines show the areas labeled with *spast* signals. Scale bar, 200 μm.

Effects of Skip *spast* Exon 6 on spinal motor neurons

An antisense oligo targeting the *spast*-E6I6-MO skipped sequence causing a frameshift mutation and the production of a termination codon were designed and injected into 1-cell stage embryos to investigate the function of *spast* in zebrafish (Fig. 5A). Different doses of *spast*-MO caused significant mortality and malformation at 2 dpf (Fig. 5B). RT−PCR analysis verified the knockdown efficiency of *spast* morpholino injection (Fig. 5C). Notably, *spast*-MO produced truncated motor axons and missed spinal motor neuron phenotypes in *Tg(hb9:GFP)*-fertilized embryos at 3 dpf compared with *std*-MO injection (Fig. 5D). Moreover, the motor neurons of 3 dpf larvae exhibited axon pathfinding defects and aberrant motor axon branching in the spinal cord (Fig. 5E). The number of spinal motor neuron axon defects in the *spast*-MO group was greater than that in the *std*-MO group, and the fluorescence intensity was lower in the spinal cords of *spast*-MO larvae than in those of *std*-MO-injected zebrafish (Fig. 5F). At 4 dpf, *spast*-MO larvae showed locomotor preference in swimming trajectory, swimming along the edge inside the wells of the 24-well plate (Fig. 5G and I); however, there was no significant difference in the total distance traveled or the movement speed between *spast*-MO larvae and *std*-MO larvae (Fig. 4S). Surprisingly, both the maximum and minimum accelerations of *spast*-MO larvae were greater than those of *std*-MO larvae (Fig. 5F).

Spast-knockdown zebrafish exhibited motor neuron defects and mild behavioral abnormalities at an early age.

(A) Schematic depiction of *spast* alteration after injection of E6I6-MO.
(B) Mortality and malformation analysis of 2 dpf larvae after 4 ng/8 ng/12 ng/16 ng morpholino injection with *spast*-MO or *std*-MO.
(C) Evaluation of the efficiency of *spast* morpholino injection at doses of 4 ng/8 ng/12 ng/16 ng by RT−PCR. ns, not statistically significant, $^{***}P \le 0.001$. $n = 3$.
(D) Expression pattern of 3 dpf *std*-MO and *spast*-MO *Tg(hb9:GFP)* larvae. Lateral views. Scale bar, 500 μm.

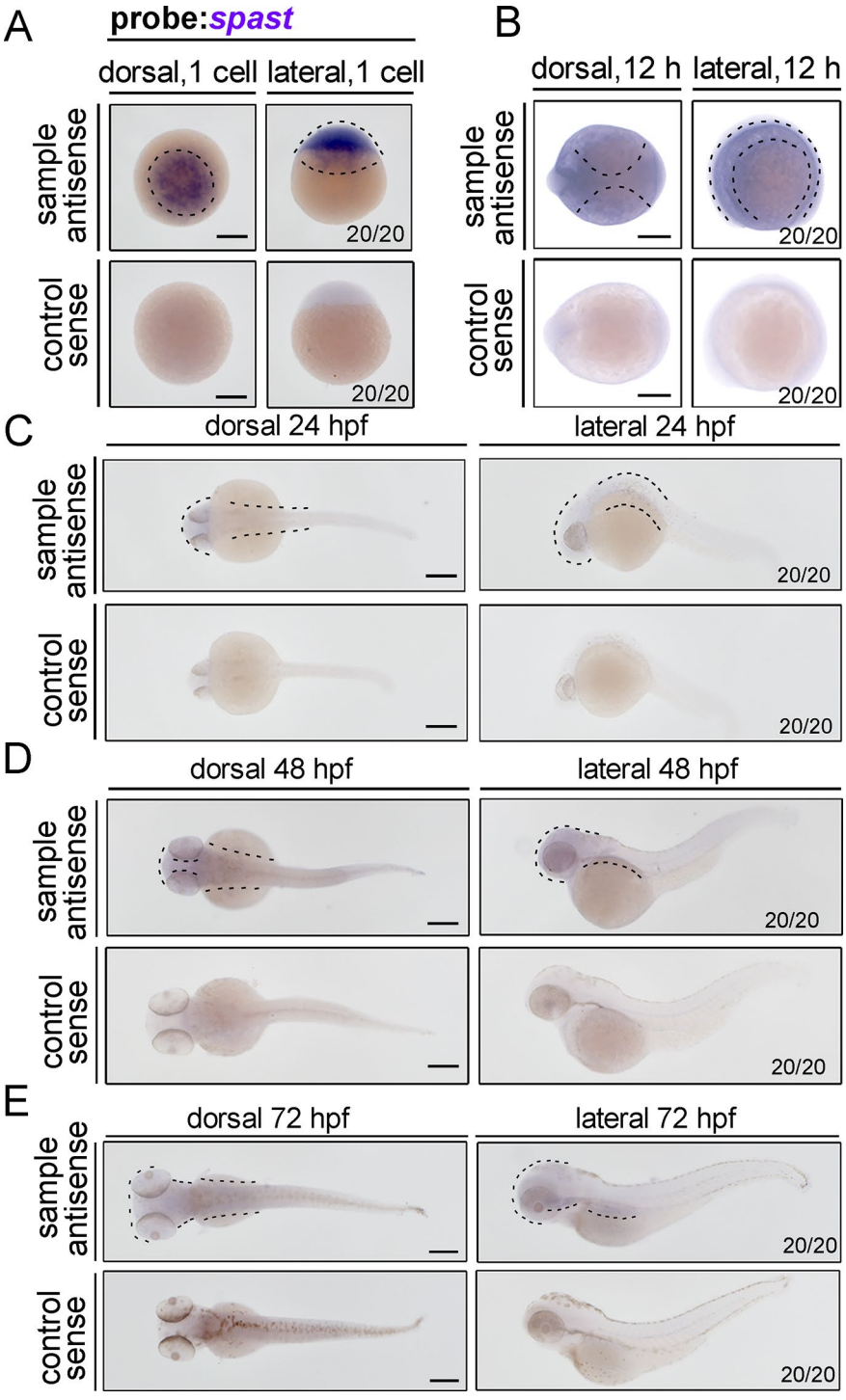

Fig. 4 Spatiotemporal expression of *spast* during zebrafish development

(E) Enlarged lateral views of the trunk in *Tg(hb9:GFP)* larvae (anterior to the left). The asterisks indicate stalled or misrouted motor neuron axons. Scale bar, 100 μm.

(F) Number of SMN axon defects and relative fluorescence intensity in (E).

(G) Movement trajectories of zebrafish larvae from the *std*-MO- and *spast*-MO-injected groups at 5 dpf. The lines represent the movement trajectories.

(H) Changes in the maximum and minimum acceleration of zebrafish larvae (F). Statistical analysis of the data of zebrafish larvae from each group. The number (n) of larvae is indicated above the

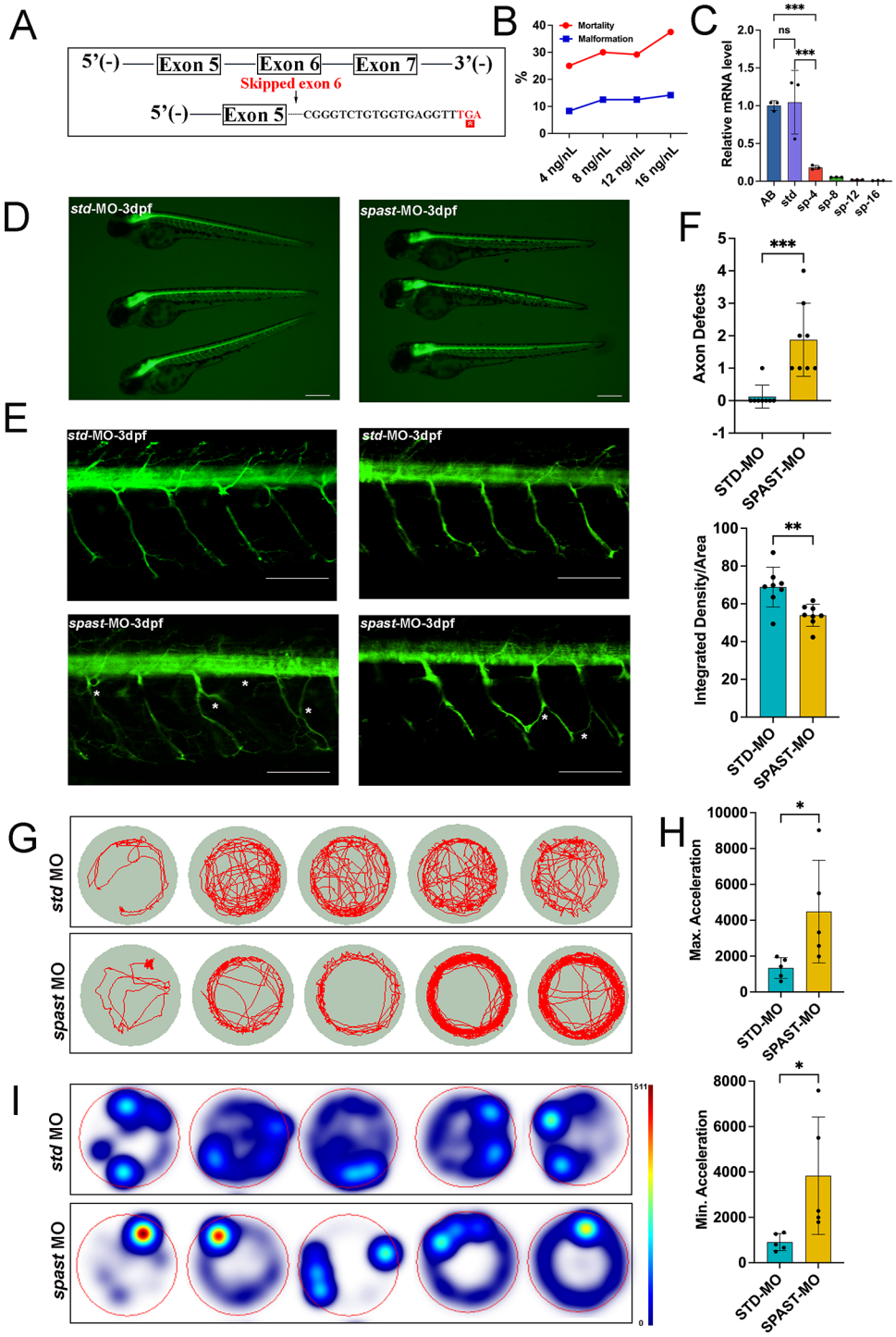

Fig. 5 *Spast* knockdown triggered motor neuron defects and behavioral dysfunction

corresponding histogram bar. The asterisks denote significant differences between the *std*-MO and *spast*-MO groups (*$P \leq 0.05$, **$P \leq 0.01$, ***$P \leq 0.001$).

(I) Heatmap showing the behavioral preference of the larvae. The longest stay time is shown in red; the medium stay time is shown in yellow, and the shortest stay time is shown in blue.

Discussion

In our study, some patients in the pedigree exhibited no additional complicated symptoms, and the manifestations of symptoms in all affected family members were less severe and appeared in a typical pure form, as observed in most cases of HSP-SPAST [10, 11]. The affected family members had similar ages of onset, at approximately thirty years. The proband's mother (II:5, 73 years old) described frequent urinary urgency. HSP-SPAST is associated with autonomic dysfunction, which may be related to the severity of the disease [25]. We reported a novel heterozygous intron variant, c.1004+5G>A, in *SPAST*. The intron splice site variant skipped exon 6, causing a frameshift mutation that resulted in a PTC.

The *SPAST* gene encodes spastin and has an open reading frame with two start codons, leading to the synthesis of two different spastin isoforms, M1 (68 kDa) and M87 (60 kDa); M87 lacks the first 86 amino acids and is expressed at significantly different levels. Spastin plays a regulatory role in microtubule severing and endoplasmic reticulum morphogenesis. Microtubules constitute a major component of the cellular cytoskeleton and are primarily composed of heterodimers of α- and β-tubulin. Microtubules serve as tracks for intracellular transport, bind to local cues to position organelles, and maintain the morphological structure of the cell [26, 27]. In neurons, microtubule stability is crucial for the transport of cargo into axons or dendrites [28]. Additionally, dysfunction in axonal transport in mature neurons has been associated with various neurodegenerative disorders, including motor neuron diseases such as amyotrophic lateral sclerosis (ALS), Alzheimer's disease (AD), and Huntington's disease (HD) [29, 30].

Various pathogenic mechanistic hypotheses for HSP-SPAST have been proposed. The haploinsufficiency hypothesis involves the inactivation of one *SPAST* allele, resulting in inadequate microtubule severing. Furthermore, a certain amount of spastin is necessary for SOCE and the maintenance of the ER structure [31]. In most studies, haploinsufficiency has been the common explanation for HSP-SPAST [32, 33]. Some data suggest a dominant negative effect as the disease-causing mechanism for HSP-SPAST, usually induced by a missense mutation in the ATPase domain of full-length spastin. This effect may occur through competition for microtubule-binding sites between the mutant and WT spastin [34] or by the interaction of the mutant protein with the WT protein to form a dysfunctional hexamer [15, 35]. Loss of spastin affects the accumulation of axonal transport cargoes, resulting in axonal swellings characterized by disorganized microtubules, mitochondria, and vesicular structures [18, 36, 37].

HSP-SPASTs exhibit various degrees of phenotypic heterogeneity, and insufficient microtubule severing cannot fully explain the symptoms [6]. Previous studies have suggested that the intracellular accumulation of mutated M1 spastin inhibits fast axonal transport (FAT) through neurotoxic effects rather than through microtubule binding or severing [38]. Notably, mutant M1 was detected in the adult thoracic spinal cord of an HSP-SPAST patient, suggesting that mutant M1 proteins may accumulate over time [39]. These findings are supported by findings in a transgenic *Spast*C448Y mouse model in which the accumulation of mutant M1 was observed in the distal axons of the corticospinal tract [40]. Crossbreeding *Spast*-KO and *hSpast*-C448Y mouse models confirmed that both gain-of-function and loss-of-function components collectively contribute to the pathogenesis of HPS-SPAST [41]. Transgenic Drosophila expressing M1 C448Y exhibit posture defects, with their wings abnormally positioned away from their bodies [42]. Gain-of-function spastin mutations affect neurite outgrowth to varying degrees, while adverse effects on microtubule dynamics lead to axonal degeneration [20].

We transiently transfected both WT and mutated plasmids into HEK293T and HeLa cells to study the simultaneous expression of the spastin M1 and M87 isoforms. Distinct mutation phenotypes were observed (Fig. 3; Fig. S3): the truncated protein was evenly distributed throughout the cytoplasm, formed filamentous accumulations around the nucleus, and colocalized with microtubules. Consistent with previous research, truncated proteins that diffused into the cytoplasm appeared denser and accumulated at microtubules around the nucleus [42]. The mutated spastin protein lacks the AAA domain, which severs microtubules. However, no abnormal microtubule structures were observed in cells transfected with mutated plasmids. Overexpression of full-length WT or mutated plasmids (both retaining two start codons in an open reading frame) in HEK293T cells mimicked in vivo conditions. We found that WT-M1 spastin was expressed at higher levels than the corresponding M87 isoform. Truncated spastin was expressed at higher levels than WT spastin.

Additionally, our study showed that the expression levels of α-tubulin did not significantly differ from those seen in WT zebrafish. To investigate the effects of the truncated protein in vivo, we generated a zebrafish model

with *spast*-MO and *spast* CRISPR/Cas9-mediated mutations. Both *spast*-MO (Fig. 5) and *spast*-F_0 crispants (Fig. S5) exhibited consistent phenotypes and developmental defects. Primarily observed motor neurons displayed axon pathfinding defects, impaired outgrowth, and axon loss. The *spast*-MO larvae exhibited unusual behavioral preferences and increased acceleration (Fig. 5). To date, katanin, spastin, and fidgetin have been shown to possess microtubule-severing activity, and appear to be involved in all major biochemical pathways in vivo. All three enzymes share a similar domain architecture, including microtubule interaction and trafficking (MIT) and ATPase, which are associated with various cellular activity (AAA) domains [43, 44]. The enzymes also share a common function in the hydrolysis of large protein polymers in the cell, such as severing microtubules [45, 46]. These findings are based on the results and most clinical pedigree features [19].

We hypothesize that in the early stage, other microtubule-severing enzymes play a partial compensatory role in maintaining normal physiological functions in the presence of haploinsufficiency. A small percentage of mutation-induced truncated *SPAST* mRNAs may escape NMD surveillance and avoid degradation [47, 48]. The truncated protein can accumulate in the spinal cord, exerting neurotoxic effects over time.

In summary, we reported a novel *SPAST* mutation. Our experimental results suggested that the primary mechanism of action was loss of function caused by insufficient levels of functional protein, and potential toxicity caused by the intracellular accumulation of spastin may be a contributing factor in HSP-SPAST. The function of spastin is not fully understood, and further studies to explore its mechanisms in response to physiological and pathological cues are warranted.

Abbreviations

HSP	Hereditary spastic paraplegia
AD	Autosomal dominant
AD	Autosomal recessive
SPG4	Spastic paraplegia type 4 (SPG4)
SOCE	Store-operated calcium entry
ER	Endoplasmic reticulum
NMD	Nonsense-mediated mRNA decay
PTCs	Premature Termination codons
PUMCH	Peking Union Medical College Hospital
PCR	Polymerase chain reaction
SPRS	Spastic Paraplegia Rating Scale
DMEM	Dulbecco's modified eagle medium
MEM	Modified eagle medium
FEB	Fetal bovine serum
PVDF	Polyvinylidene fluoride
BSA	Bovine serum albumin
DAPI	4,6-diamidino-2-phenylindole
gRNA	Guide RNA
MO	Morpholino
dpf	Days postfertilization
ANOVA	One-way analysis of variance
WT	Wild-type
ZsGreen	Zoanthus green
MIT	Microtubule interacting and trafficking domain
MBD	Microtubule-binding domain
AAA	ATPase associated with various cellular activities
hpf	Postfertilization
ALS	Amyotrophic lateral sclerosis (ALS)
AD	Alzheimer's disease
HD	Huntington's disease
FAT	Fast axonal transport

Supplementary Information

The online version contains supplementary material available at https://doi.org/10.1186/s12967-024-05669-8.

Supplementary Material 1

Acknowledgements

We would like to express our sincere gratitude to the Biomedical Engineering Facility, Institute of Clinical Medicine, Chinese Academy of Medical Sciences for providing the necessary facilities and resources for this research. Our heartfelt thanks also go to teacher Lulu Liu and her dedicated team for their invaluable guidance, support, and contributions throughout the course of this study.

Author contributions

Wan Xinhua: Conceptualization and design of the experiments. Luo Min: Validation, Investigation, Writing - Original Draft, Visualization. Wang Yanying: Investigation, Writing - Review & Editing. Liang Jinxiu: Resources.

Funding

This study was supported by National High Level Hospital Clinical Research Funding (2022-PUMCH-B-018).

Data availability

All the data are presented in this manuscript and supplemental material.

Declarations

Consent for publication

All the authors agree to publish this study.

Competing interests

The authors declare that they have no known competing financial interests or personal relationships that could have appeared to influence the work reported in this paper.

Received: 7 April 2024 / Accepted: 10 September 2024
Published online: 27 September 2024

References

1. Shribman S, Reid E, Crosby AH, Houlden H, Warner TT. Hereditary spastic paraplegia: from diagnosis to emerging therapeutic approaches. Lancet Neurol. 2019;1812. https://doi.org/10.1016/s1474-4422(19)30235-2.
2. Panza E, Meyyazhagan A, Orlacchio A. Hereditary spastic paraplegia: genetic heterogeneity and common pathways. Exp Neurol. 2022;357. https://doi.org/10.1016/j.expneurol.2022.114203.
3. Meyyazhagan A, Orlacchio A. Hereditary Spastic Paraplegia: an update. Int J Mol Sci. 2022;233. https://doi.org/10.3390/ijms23031697.
4. Fereshtehnejad SM, Saleh PA, Oliveira LM, Patel N, Bhowmick S, et al. Movement disorders in hereditary spastic paraplegia (HSP): a systematic review and individual participant data meta-analysis. Neurol Sci. 2023;443. https://doi.org/10.1007/s10072-022-06516-8.
5. Erfanian Omidvar M, Torkamandi S, Rezaei S, Alipoor B, Omrani MD, et al. Genotype-phenotype associations in hereditary spastic paraplegia: a systematic review and meta-analysis on 13,570 patients. J Neurol. 2021;2686. https://doi.org/10.1007/s00415-019-09633-1.
6. Schüle R, Wiethoff S, Martus P, Karle KN, Otto S, et al. Hereditary spastic paraplegia: clinicogenetic lessons from 608 patients. Ann Neurol. 2016;794. https://doi.org/10.1002/ana.24611.

7. Yu W, He J, Liu X, Wu J, Cai X, et al. Clinical features and genetic spectrum of Chinese patients with hereditary spastic paraplegia: a 14-year study. Front Genet. 2023;14. https://doi.org/10.3389/fgene.2023.1085442.
8. Ruano L, Melo C, Silva MC, Coutinho P. The global epidemiology of hereditary ataxia and spastic paraplegia: a systematic review of prevalence studies. Neuroepidemiology. 2014;423. https://doi.org/10.1159/000358801.
9. Cunha IA, Ribeiro JA, Santos MC. Hereditary spastic paraparesis: the real-world experience from a Neurogenetics outpatient clinic. Eur J Med Genet. 2022;653. https://doi.org/10.1016/j.ejmg.2022.104430.
10. Méreaux JL, Banneau G, Papin M, Coarelli G, Valter R, et al. Clinical and genetic spectra of 1550 index patients with hereditary spastic paraplegia. Brain. 2022;1453. https://doi.org/10.1093/brain/awab386.
11. Cao Y, Zheng H, Zhu Z, Yao L, Tian W, et al. Clinical and genetic spectrum in a large cohort of Hereditary Spastic Paraplegia. Mov Disord. 2024. https://doi.org/10.1002/mds.29728.
12. Varghaei P, Estiar MA, Ashtiani S, Veyron S, Mufti K, et al. Genetic, structural and clinical analysis of spastic paraplegia 4. Parkinsonism Relat Disord. 2022;98. https://doi.org/10.1016/j.parkreldis.2022.03.019.
13. Navas-Sánchez FJ, Fernández-Pena A, Martín de Blas D, Alemán-Gómez Y, Marcos-Vidal L, et al. Thalamic atrophy in patients with pure hereditary spastic paraplegia type 4. J Neurol. 2021;2687. https://doi.org/10.1007/s00415-020-10387-4.
14. Lo Giudice T, Lombardi F, Santorelli FM, Kawarai T, Orlacchio A. Hereditary spastic paraplegia: clinical-genetic characteristics and evolving molecular mechanisms. Exp Neurol. 2014;261. https://doi.org/10.1016/j.expneurol.2014.06.011.
15. Shoukier M, Neesen J, Sauter SM, Argyriou L, Doerwald N, et al. Expansion of mutation spectrum, determination of mutation cluster regions and predictive structural classification of SPAST mutations in hereditary spastic paraplegia. Eur J Hum Genet. 2009;172. https://doi.org/10.1038/ejhg.2008.147.
16. White SR, Evans KJ, Lary J, Cole JL, Lauring B. Recognition of C-terminal amino acids in tubulin by pore loops in Spastin is important for microtubule severing. J Cell Biol. 2007;1767. https://doi.org/10.1083/jcb.200610072.
17. Tadepalle N, Robers L, Veronese M, Zentis P, Babatz F, et al. Microtubule-dependent and independent roles of spastin in lipid droplet dispersion and biogenesis. Life Sci Alliance. 2020;36. https://doi.org/10.26508/lsa.202000715.
18. Rizo T, Gebhardt L, Riedlberger J, Eberhardt E, Fester L, et al. Store-operated calcium entry is reduced in spastin-linked hereditary spastic paraplegia. Brain. 2022;1459. https://doi.org/10.1093/brain/awac122.
19. Chen R, Du S, Yao Y, Zhang L, Luo J, et al. A novel SPAST mutation results in Spastin Accumulation and defects in Microtubule Dynamics. Mov Disord. 2022;373. https://doi.org/10.1002/mds.28885.
20. Solowska JM, Baas PW. Hereditary spastic paraplegia SPG4: what is known and not known about the disease. Brain. 2015;138. https://doi.org/10.1093/brain/awv178.
21. Dyle MC, Kolakada D, Cortazar MA, Jagannathan S. How to get away with nonsense: mechanisms and consequences of escape from nonsense-mediated RNA decay. Wiley Interdiscip Rev RNA. 2020;111. https://doi.org/10.1002/wrna.1560.
22. Sato H, Singer RH. Cellular variability of nonsense-mediated mRNA decay. Nat Commun. 2021;121. https://doi.org/10.1038/s41467-021-27423-0.
23. Schüle R, Holland-Letz T, Klimpe S, Kassubek J, Klopstock T, et al. The spastic Paraplegia Rating Scale (SPRS): a reliable and valid measure of disease severity. Neurology. 2006;673. https://doi.org/10.1212/01.wnl.0000228242.53336.90.
24. Thisse C, Thisse B. High-resolution in situ hybridization to whole-mount zebrafish embryos. Nat Protoc. 2008;31. https://doi.org/10.1038/nprot.2007.514.
25. González-Salazar C, Takazaki KAG, Martinez ARM, Pimentel-Silva LR, Jacinto-Scudeiro LA, et al. Autonomic dysfunction in hereditary spastic paraplegia type 4. Eur J Neurol. 2019;264. https://doi.org/10.1111/ene.13878.
26. Kapitein LC. and C. C. Hoogenraad. Building the neuronal Microtubule Cytoskeleton. Neuron 2015. 873. https://doi.org/10.1016/j.neuron.2015.05.046
27. Cushion TD, Leca I, Keays DA. MAPping tubulin mutations. Front Cell Dev Biol. 2023;11. https://doi.org/10.3389/fcell.2023.1136699.
28. Sheetz MP, Steuer ER, Schroer TA. The mechanism and regulation of fast axonal transport. Trends Neurosci. 1989;1211. https://doi.org/10.1016/0166–2236(89)90099-4.
29. White JA, Banerjee R, Gunawardena S. Axonal Transport and neurodegeneration: how Marine drugs can be used for the development of therapeutics. Mar Drugs. 2016;145. https://doi.org/10.3390/md14050102.
30. Zempel H, Mandelkow EM. Tau missorting and spastin-induced microtubule disruption in neurodegeneration: Alzheimer Disease and Hereditary Spastic Paraplegia. Mol Neurodegener. 2015;10. https://doi.org/10.1186/s13024-015-0064-1.
31. Julien C, Lissouba A, Madabattula S, Fardghassemi Y, Rosenfelt C, et al. Conserved pharmacological rescue of hereditary spastic paraplegia-related phenotypes across model organisms. Hum Mol Genet. 2016;256. https://doi.org/10.1093/hmg/ddv632.
32. Roll-Mecak A, Vale RD. Structural basis of microtubule severing by the hereditary spastic paraplegia protein spastin. Nature. 2008;4517176. https://doi.org/10.1038/nature06482.
33. Schickel J, Beetz C, Frömmel C, Heide G, Sasse A, et al. Unexpected pathogenic mechanism of a novel mutation in the coding sequence of SPG4 (spastin). Neurology. 2006;663. https://doi.org/10.1212/01.wnl.0000196468.01815.55.
34. McDermott CJ, Grierson AJ, Wood JD, Bingley M, Wharton SB, et al. Hereditary spastic paraparesis: disrupted intracellular transport associated with spastin mutation. Ann Neurol. 2003;546. https://doi.org/10.1002/ana.10757.
35. Pantakani DV, Swapna LS, Srinivasan N, Mannan AU. Spastin oligomerizes into a hexamer and the mutant spastin (E442Q) redistribute the wild-type spastin into filamentous microtubule. J Neurochem. 2008;1062. https://doi.org/10.1111/j.1471-4159.2008.05414.x.
36. Sardina F, Pisciottani A, Ferrara M, Valente D, Casella M, et al. Spastin recovery in hereditary spastic paraplegia by preventing neddylation-dependent degradation. Life Sci Alliance. 2020;312. https://doi.org/10.26508/lsa.202000799.
37. Denton KR, Lei L, Grenier J, Rodionov V, Blackstone C, et al. Loss of spastin function results in disease-specific axonal defects in human pluripotent stem cell-based models of hereditary spastic paraplegia. Stem Cells. 2014;322. https://doi.org/10.1002/stem.1569.
38. Leo L, Weissmann C, Burns M, Kang M, Song Y, et al. Mutant spastin proteins promote deficits in axonal transport through an isoform-specific mechanism involving casein kinase 2 activation. Hum Mol Genet. 2017;2612. https://doi.org/10.1093/hmg/ddx125.
39. Solowska JM, Garbern JY, Baas PW. Evaluation of loss of function as an explanation for SPG4-based hereditary spastic paraplegia. Hum Mol Genet. 2010;1914. https://doi.org/10.1093/hmg/ddq177.
40. Qiang L, Piermarini E, Muralidharan H, Yu W, Leo L, et al. Hereditary spastic paraplegia: gain-of-function mechanisms revealed by new transgenic mouse. Hum Mol Genet. 2019;287. https://doi.org/10.1093/hmg/ddy419.
41. Piermarini E, Akarsu S, Connors T, Kneussel M, Lane MA, et al. Modeling gain-of-function and loss-of-function components of SPAST-based hereditary spastic paraplegia using transgenic mice. Hum Mol Genet. 2022;3111. https://doi.org/10.1093/hmg/ddab367.
42. Solowska JM, D'Rozario M, Jean DC, Davidson MW, Marenda DR, et al. Pathogenic mutation of spastin has gain-of-function effects on microtubule dynamics. J Neurosci. 2014;345. https://doi.org/10.1523/jneurosci.3309-13.2014.
43. Zehr E, Szyk A, Piszczek G, Szczesna E, Zuo X, et al. Katanin spiral and ring structures shed light on power stroke for microtubule severing. Nat Struct Mol Biol. 2017;249. https://doi.org/10.1038/nsmb.3448.
44. McNally FJ, Roll-Mecak A. Microtubule-severing enzymes: from cellular functions to molecular mechanism. J Cell Biol. 2018;21712. https://doi.org/10.1083/jcb.201612104.
45. Shin SC, Im SK, Jang EH, Jin KS, Hur EM, et al. Structural and molecular basis for katanin-mediated severing of Glutamylated Microtubules. Cell Rep. 2019;265. https://doi.org/10.1016/j.celrep.2019.01.020.
46. Kuo YW, Howard J. Cutting, amplifying, and aligning microtubules with severing enzymes. Trends Cell Biol. 2021;311. https://doi.org/10.1016/j.tcb.2020.10.004.
47. Claudiani P, Riano E, Errico A, Andolfi G, Rugarli EI. Spastin subcellular localization is regulated through usage of different translation start sites and active export from the nucleus. Exp Cell Res. 2005;3092. https://doi.org/10.1016/j.yexcr.2005.06.009.
48. Nan H, Chu M, Liu L, Xie K, Wu L. A novel truncating variant of SPAST associated with hereditary spastic paraplegia indicates a haploinsufficiency pathogenic mechanism. Front Neurol. 2022;13. https://doi.org/10.3389/fneur.2022.1005544.

Publisher's note